Postprint of: Kumar Jena S., Chakraverty S., Malikan M.: Implementation of Non-Probabilistic Methods for Stability Analysis of Nonlocal Beam with Structural Uncertainties. ENGINEERING WITH COMPUTERS. (2020). DOI: 10.1007/s00366-020-00987-z

Implementation of Non-Probabilistic Methods for Stability Analysis of Nonlocal Beam with Structural Uncertainties

Subrat Kumar Jena[1], S. Chakraverty[2]*, Mohammad Malikan[3]

[1, 2]Department of Mathematics, National Institute of Technology Rourkela, 769008, India

[3]Department of Mechanics of Materials and Structures, Faculty of Civil and Environmental Engineering, Gdansk University of Technology, 80-233, ul. G. Narutowicza 11/12, Gdansk, Poland

*Corresponding author

E-mail: [1]sjena430@gmail.com, [2]sne_chak@yahoo.com, [3] mohammad.malikan@pg.edu.pl

Abstract

In this study, a non-probabilistic approach based Navier's Method (NM) and Galerkin Weighted Residual Method (GWRM) in term of double parametric form has been proposed to investigate the buckling behavior of Euler-Bernoulli nonlocal beam under the framework of the Eringen's nonlocal elasticity theory, considering the structural parameters as imprecise or uncertain. The uncertainties in Young's modulus and diameter of the beam are modeled in terms of Triangular Fuzzy Numbers (TFN). The critical buckling loads are calculated for Hinged-Hinged (HH), Clamped-Hinged (CH), and Clamped-Clamped (CC) boundary conditions and these results are compared with the deterministic model in special cases, demonstrating robust agreement. Further, a random sampling technique based method namely, Monte Carlo Simulation Technique (MCST) has been implemented to compute the critical buckling loads of uncertain systems. Also, the critical buckling loads obtained from the uncertain model in terms of Lower Bound (LB) and

Upper Bound (UB) by the non-probabilistic methods, viz. Navier's Method (NM) and Galerkin Weighted Residual Method (GWRM), are again verified with the Monte Carlo Simulation Technique (MCST) with their time periods, demonstrating the efficacy, accuracy, and effectiveness of the proposed uncertain model. A comparative study is also carried out among the non-probabilistic methods and Monte Carlo Simulation Technique (MCST) to demonstrate the effectiveness of methods with respect to time. Additionally, a parametric study has been performed to display the propagation of uncertainties into the nonlocal system in the form of critical buckling loads.

Keywords

Monte Carlo Simulation Technique; Navier's Method; Galerkin Weighted Residual Method; Critical Buckling Load; Structural Uncertainties; Triangular Fuzzy Number.

1. Introduction

Probabilistic and non-probabilistic methods are the ones that have been being used in mathematics as well as in mechanical and civil engineering in order to predict the mechanical behavior of materials with deterministic and uncertain properties. The probabilistic method [1-2] was initially utilized in combinatorics in order to approve a special type of mathematical object. This shows that if one accidentally selects objects from a given class, the probability of the result being of the prescribed type is significantly greater than zero. However, the mathematical process uses probability, the final result is determined certainly and there are no probable errors. Some of the applications of probabilistic techniques can be seen in mathematics, in particular, real analysis, number theory, and linear algebra, etc. It can also be used in information theory and randomized rounding in computer science areas [3]. On the other hand, non-probabilistic methods such as the Navier's method [4-6] and Galerkin weighted residual method [7-8], have been used extensively in mathematics and mechanics, particularly solid mechanics. These methods depend on deterministic values instead of random or uncertain values. In fact, these methods carry out problems based on perception and observation.

Uncertainties in structural properties can occur due to various factors such as environmental conditions, measurement errors, defects in atomic structures, etc. As a matter of fact, these anomalies in structural properties designate that the materials might not have the ability to indicate its normal mechanical behavior. Additionally, the effects of uncertainties in case of nonlocal

structures will become much more profound because of small scale effects [9-11]. Due to the widespread applicability of nanostructures in various sensitive and sophisticated devices, the modeling of nanostructures considering material uncertainties are now becoming very essential as the impacts of uncertainties influence the static and dynamic characteristics very adversely. In this context, various works have been carried out in recent years related to structural uncertainties. Radebe and Adali [12] estimated material uncertainty for an orthotropic nanoscale plate subjected to stability conditions. Lv and Liu studied uncertainties about a functionally graded nanobeam under bending [13] and thermo-modal [14] analyses. Furthermore, Liu and Lv [15] investigated material uncertainties for a nanobeam under wave dispersion analysis while a piezoelectric/magnetic nanobeam was exposed to electro-magneto-mechanical stress fields. In other considerations, Liu and Lv modeled a carbon nanotube when material uncertainties were also taken into account in eigenvalues [16] and frequency [17] considerations. Jena et al. [18] investigated the propagation of uncertainty in frequency parameters of an Euler-Bernoulli nonlocal beam. Gironacci et al. [19] modeled crack propagation for a nonlocal domain whilst uncertain material properties were also considered. Zhu et al. [20] studied natural frequencies of a nanoscale plate that their study also included material uncertainties within which the material was affected by thermal and electrical environments.

In the pioneering work [21], Karami and Shahsavari investigated forced resonant vibration of doubly-curved nanoshells made up of functionally graded polymer composite considering four different geometries such as spherical, elliptical, hyperbolic and cylindrical. Karami et al. [22] studied free vibration characteristics of non-uniform Timoshenko nanobeam composed of functionally graded materials in the thermal environment. Here, the size-dependent effect of the nanobeam was captured by the nonlocal strain gradient model. Karami et al. [23] used higher-order shear deformation shell theory in conjunction with nonlocal strain gradient theory to analyze dispersion characteristics of elastic eaves in doubly curved nanoshells composed of functionally graded anisotropic materials. Bi-Helmholtz nonlocal strain gradient theory has been used to investigate elastic buck wave characteristics of functionally graded anisotropic doubly curved nanoshells [24] and resonance behavior of Kirchhoff nanoplates [25]. Karami et al. [26] again analyzed static behavior functionally graded nanoplates composed of hexagonal beryllium crystals using five variables refined plate theory in association with nonlocal strain gradient theory. Lyu et al. [27] implemented a hull iteration method to investigate the impact of nano-system uncertainties

on the critical flow velocity of fluid carrying carbon nanotubes positioned in an elastic matrix and exposed to the thermal and magnetic condition. The nonlocal effect of the system was captured by Eringen's nonlocal elasticity theory. Liu et al. studied the nonlinear vibration of functionally graded sandwich nanobeams [28] and nonlinear dynamic response of an FG multilayer beam [29] with initial geometric imperfection while the size-dependent effect was analyzed by nonlocal strain gradient theory.

Malikan and Eremeyev [30] exploited the Rayleigh-Ritz method to investigate the post-buckling behavior of truncated conical carbon nanotubes placed in a nonlinear elastic foundation considering surface effect under the framework Euler-Bernoulli beam theory and nonlocal strain gradient theory. Malikan et al. [31] analyzed the torsional stability of the nono-composite shell based on first-order shear deformation shell theory and nonlocal strain gradient theory subjected to the three-dimensional magnetic field. Jena et al. [32] investigate the dynamical behavior of nanobeam embedded in a Winkler-Pasternak elastic substrate subjected to an axial magnetic field based on a refined beam theory in conjunction with Eringen's nonlocal model and the Navier's approach has been used to compute the closed-form solution. Jena et al. [33] again analyzed the buckling behavior of zigzag, chiral, and armchair types of single-walled carbon nanotubes embedded in the Winkler elastic foundation subjected to low and high-temperature environments considering the effect of surface energy and surface residual stresses. Vibration and buckling characteristics of electromagnetic nanobeam using Higher-Order Haar Wavelet Method and shifted Chebyshev polynomial based Rayleigh-Ritz method are studied by Jena and Chakraverty [34] and Jena et al. [35], respectively. Jena et al. [36] conducted a comparative study to find out buckling response analysis of strain gradient nonlocal beam by using Haar wavelet, higher-order Haar wavelet, and differential quadrature methods. In the work [37], Jena et al. used a novel fractional nonlocal elasticity theory to predict the buckling behavior of Euler-Bernoulli nanobeam using differential quadrature method. Jena et al. also analyzed the vibration characteristics of Euler-Bernoulli nanobeam placed on the variable elastic foundation [38-39] using the differential quadrature method. Some other works related to nanostructure with respect to differential quadrature method, varying elastic foundation, etc. can be found in [40-48].

Based on the extent and nature of the uncertainties indicated in any domain, there are some techniques to analyze the uncertainty. First, the factors of a system have behaved randomly under determined distributions of probability. So, in this case, the outcomes of the system should be

expressed randomly based on the probability theory. Moreover, if a part of information about the uncertainty has existed, the upper bound should be made on the system's utmost outcome by means of the anti-optimization technique. In addition, if the parameters of the system are defined imprecisely, the theory of Fuzzy should be exploited. Zadeh [49] was the first to propose the basic theoretical concepts of fuzzy. Based on this concept, several works have been carried out in solid mechanics [50-53]. For more basic concepts of fuzzy and its application to various engineering problems, one may refer [54-56].

As it turned out, the studies on nanostructural material uncertainties are limited, therefore, the present study is devoted to investigating the propagation of material uncertainties into the buckling characteristics of the nonlocal beam using non-probabilistic methods such as double parametric form-based Navier's method and Galerkin weighted residual method as well as random sampling technique based Monte Carlo simulation technique. To model and simulate the motion of nodes of the beam, the Euler-Bernoulli beam theory is employed considering the diameter of the beam and the elasticity modulus of the material as uncertain by means of Triangular Fuzzy Numbers (TFN). The numerical results are presented for different boundary conditions, namely Clamped-Clamped (CC), Hinged-Hinged (HH), and Clamped-Hinged (CH). Thereafter, the numerical outcomes are compared among the Monte Carlo simulation technique and non-probabilistic methods. Furthermore, a fully parametric study is conducted considering the effects of uncertainties on critical buckling loads.

2. Preliminaries [18, 49, 53-56]

Fuzzy Set: A fuzzy set $\widetilde{S}$ is a set of ordered pairs where the first element (s) of order pair belongs to the universal set (U) and the second element is assigned to a value, namely membership values $\mu(s)$ which is denoted as

$$\widetilde{S} = \{(s,\ \mu(s)) :\ s \in U,\ \mu(s) \in [0,\ 1]\} \tag{1}$$

Fuzzy Number: A fuzzy number $\widetilde{S}$ is defined as a convex normalized fuzzy set $\widetilde{S}$ of R such that

$$\left\{ \mu_{\widetilde{S}}(s) : R \to [0,\ 1], \forall\, s \in R \right\} \tag{2}$$

where $\mu_{\widetilde{S}}$ is the membership function of the fuzzy set which is piecewise continuous.

Triangular Fuzzy Number(TFN): A triangular fuzzy number $\tilde{S} = (s_1, s_2, s_3)$ is defined as a convex normalized fuzzy set $\tilde{S}$ of the real line R, the schematic diagram is illustrated in Fig. 1, such that the membership function $\mu_{\tilde{S}}$ of $\tilde{S}$ given as

$$\mu_{\tilde{S}}(s) = \begin{cases} 0, & s \le s_1 \\ \dfrac{s - s_1}{s_2 - s_1}, & s_1 \le s \le s_2 \\ \dfrac{s_3 - s}{s_3 - s_2}, & s_2 \le s \le s_3 \\ 0, & s \ge s_3. \end{cases} \tag{3}$$

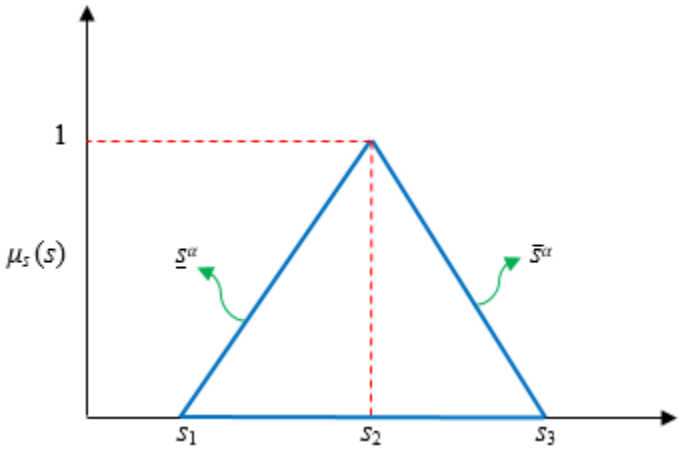

Fig. 1: Graphical representation of Triangular Fuzzy Number $\tilde{S} = (s_1, s_2, s_3)$

Single Parametric Form: A triangular fuzzy number $\tilde{S} = (s_1, s_2, s_3)$ can be transformed to an interval of ordered pair through α cut as

$$\tilde{S}(\alpha) = \left[\underline{s}^{\alpha},\ \bar{s}^{\alpha}\right] = \left[(s_2 - s_1)\alpha + s_1,\ -(s_3 - s_2)\alpha + s_3\right], \text{ where } \alpha \in [0,1]. \tag{4}$$

Double Parametric Form: It is already mentioned above that the triangular fuzzy number $\tilde{S} = (s_1, s_2, s_3)$ can be transformed into an interval $\tilde{S}(\alpha) = \left[\underline{s}^{\alpha},\ \bar{s}^{\alpha}\right]$ by using α cut approach. Further, the interval $\tilde{S}(\alpha) = \left[\underline{s}^{\alpha},\ \bar{s}^{\alpha}\right]$ can be written as

$$\tilde{S}(\alpha,\ \beta) = \left(\bar{s}^{\alpha} - \underline{s}^{\alpha}\right)\beta + \underline{s}^{\alpha}, \text{ where } \alpha, \beta \in [0\ 1]. \tag{5}$$

3. Mathematical formulation

In this section, the governing equation for the stability analysis of the nanobeam has been developed by considering the material uncertainties associated with Young's modulus and the diameter of the nanobeam in terms of Triangular Fuzzy Number. The double parametric form is also implemented to derive the governing equation with structural uncertainties.

3.1 Governing Equation of Motion with Structural Uncertainties

The equation of motion for the buckling of Euler-Bernoulli beam in term of bending moment and transverse displacement may be expressed as [57]

$$\frac{d^2M}{dx^2} = \hat{P}\frac{d^2w}{dx^2} \tag{6}$$

In which, M is the bending moment and $\hat{P}$ is the applied compressive force due to mechanical load. The nonlocal constitutive relation, by implementing Eringen's nonlocal elasticity theory [58] may be expressed as [57]

$$M^{nl} - (e_0 a)^2 \frac{d^2M}{dx^2} = -EI\frac{d^2w}{dx^2} \tag{7}$$

Where E, I, and $(e_0 a)^2$ represent Young's modulus, second moment of area and small scale parameter of the beam, respectively.

Using Eq. (6) into Eq. (7) and simplifying, we obtain

$$M^{nl} = -EI\frac{d^2w}{dx^2} + (e_0 a)^2\left(\hat{P}\frac{d^2w}{dx^2}\right) \tag{8}$$

In this study, both Young's modulus and the diameter of the beam are considered as uncertain or random in terms of Triangular Fuzzy Number (TFN). Therefore, the uncertain Young's modulus and diameter can be expressed as

$$\tilde{E} = (e_1, e_2, e_3) \text{ and } \tilde{d} = (d_1, d_2, d_3) \tag{9}$$

In which d_2 and e_2 represent deterministic values of Young's modulus and diameter of the beam, respectively. The graphical representation of the uncertain Young's modulus and diameter are demonstrated in Fig. 2 and Fig. 3, respectively.

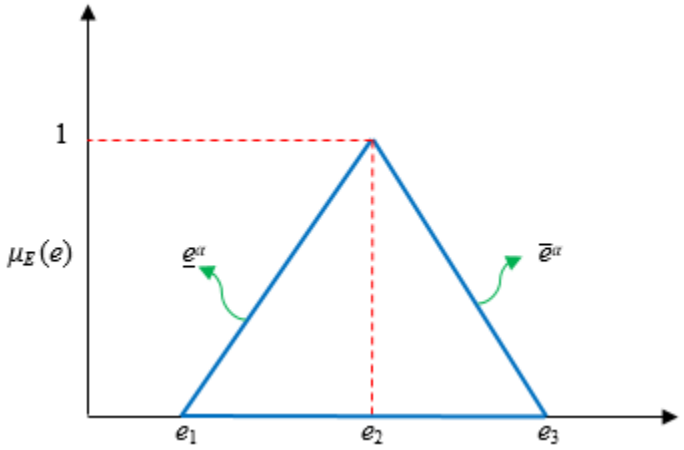

Fig. 2: Graphical representation of $\tilde{E} = (e_1, e_2, e_3)$

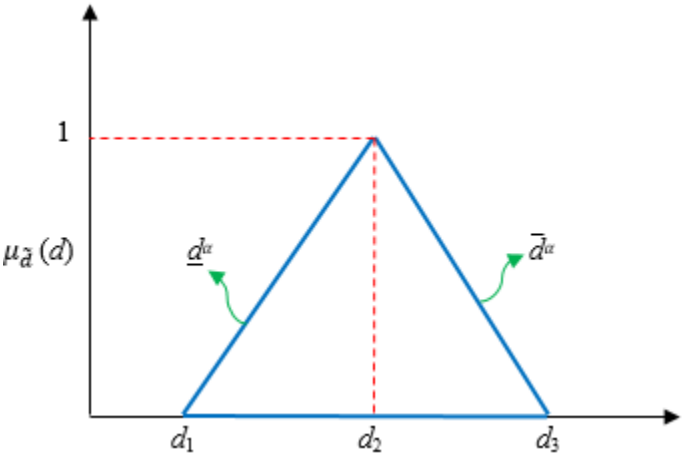

Fig. 3: Graphical representation of $\tilde{d} = (d_1, d_2, d_3)$

Plugging Eq. (9) into Eq. (8), we have

$$M^{nl} = -\tilde{E}\frac{\pi\tilde{d}^4}{64}\frac{d^2w}{dx^2} + (e_0 a)^2\left(\hat{P}\frac{d^2w}{dx^2}\right) \tag{10}$$

Using Eq. (10) in Eq. (6), the governing equation of motion for stability analysis of nonlocal beam considering the uncertainties in Young's modulus and diameter can be expressed as

$$-\tilde{E}\frac{\pi\tilde{d}^4}{64}\frac{d^4w}{dx^4} + (e_0 a)^2\hat{P}\frac{d^4w}{dx^4} - \hat{P}\frac{d^2w}{dx^2} = 0 \tag{11}$$

Incorporating the concept of the double parametric form given in Eq.(4) and Eq.(5), the triangular fuzzy numbers $\tilde{E} = (e_1, e_2, e_3)$ and $\tilde{d} = (d_1, d_2, d_3)$ can be expressed in double parametric form as

$$\tilde{E}(\alpha_1, \beta_1) = (e_1 - e_3)\alpha_1\beta_1 + (e_3 - e_1)\beta_1 + (e_2 - e_1)\alpha_1 + e_1, \quad \alpha_1, \beta_1 \in [0\ 1] \tag{12}$$

$$\tilde{d}(\alpha_2, \beta_2) = (d_1 - d_3)\alpha_2\beta_2 + (d_3 - d_1)\beta_2 + (d_2 - d_1)\alpha_2 + d_1, \quad \alpha_2, \beta_2 \in [0\ 1] \tag{13}$$

Plugging Eq.(12) and Eq.(13) in Eq.(11), the governing Eq.(11) can be modified into

$$-\tilde{E}(\alpha_1, \beta_1)\frac{\pi}{64}\left(\tilde{d}(\alpha_2, \beta_2)\right)^4 \frac{d^4w}{dx^4} + (e_0a)^2 \hat{P}\frac{d^4w}{dx^4} - \hat{P}\frac{d^2w}{dx^2} = 0 \tag{14}$$

4. Solution Procedure

In this study, three methods such as Navier's method, Galerkin weighted residual method and Monte Carlo simulation technique have been utilized to find out the critical buckling loads of Euler-Bernoulli nanobeam having structural uncertainties. Navier's method has been used for Hinged-Hinged (HH) boundary condition whereas Galerkin weighted residual method has been employed for Clamped-Hinged (CH) and Clamped-Clamped (CC) boundary conditions, based on the double parametric approach of triangular fuzzy number. Monte Carlo simulation technique is also used for all the boundary conditions after converting the triangular fuzzy number into interval form.

4.1 Navier's Method

Navier's approach has been employed to compute the critical buckling loads of nanobeam with structural uncertainties analytically, for Hinged- Hinged (HH) boundary condition. The transverse displacement (w) may be expressed as [4, 5, 6]

$$w(x) = \sum_{n=1}^{\infty} W_n \sin\left(\frac{n\pi}{L}x\right) \tag{15}$$

In which W_n is the unknown to be determined. Plugging Eq. (15) into Eq. (14), the buckling load $\left(\hat{P}_n\right)$ may be obtained as

$$\hat{P}_n = \frac{\tilde{E}(\alpha_1, \beta_1)\frac{\pi}{64}\left(\tilde{d}(\alpha_2, \beta_2)\right)^4\left(\frac{n\pi}{L}\right)^4}{\left(\frac{n\pi}{L}\right)^2 + (e_0a)^2\left(\frac{n\pi}{L}\right)^4} \tag{16}$$

Now, by using the double parametric form for Young's modulus and diameter, the above equation will be modified into

$$\hat{P}_n = \frac{\left[\begin{array}{l}\left(\left(e_1-e_3\right)\alpha_1\beta_1+\left(e_3-e_1\right)\beta_1+\left(e_2-e_1\right)\alpha_1+e_1\right)\times \\ \left(\left(d_1-d_3\right)\alpha_2\beta_2+\left(d_3-d_1\right)\beta_2+\left(d_2-d_1\right)\alpha_2+d_1\right)^4\end{array}\right]\left(\frac{\pi}{64}\right)\left(\frac{n\pi}{L}\right)^4}{\left(\frac{n\pi}{L}\right)^2+\left(e_0a\right)^2\left(\frac{n\pi}{L}\right)^4} \tag{17}$$

Putting $n=1,2,3$ etc., we will obtain critical buckling load, second buckling load, third buckling load, etc.

4.2 Galerkin Weighted Residual Method

In this section, a double parametric form-based Galerkin weighted residual method has been used to compute critical buckling loads for Clamped-Hinged (CH) and Clamped-Clamped (CC) boundary conditions. For the exact solution, the right-hand side of Eq. (14) is zero whereas the right-hand side of the Eq. (14) is not exactly zero in case of the approximate solution. So, the residue of the Eq. (14) can be defined as

$$\Re = -\tilde{\tilde{E}}\left(\alpha_1,\beta_1\right)\frac{\pi}{64}\left(\tilde{\tilde{d}}\left(\alpha_2,\beta_2\right)\right)^4\frac{d^4w}{dx^4}+\left(e_0a\right)^2\hat{P}\frac{d^4w}{dx^4}-\hat{P}\frac{d^2w}{dx^2} \tag{18}$$

The transverse displacement function w is approximated by a weighting function Φ_n as

$$w=\sum_{n=1}^{\infty}w_n\Phi_n\left(x\right) \tag{19}$$

Here, w_n is the unknown coefficient and the function $\Phi_n\left(x\right)$ has different values for different boundary conditions which are given as below[7, 20];

Clamped-Hinged (CH):

$$\Phi_n\left(x\right)=\left\langle\begin{array}{l}\sin\left(\frac{\left(n+0.25\right)\pi}{L}x\right)-\sinh\left(\frac{\left(n+0.25\right)\pi}{L}x\right)- \\ \xi_n\left[\cos\left(\frac{\left(n+0.25\right)\pi}{L}x\right)-\cosh\left(\frac{\left(n+0.25\right)\pi}{L}x\right)\right]\end{array}\right\rangle \tag{20}$$

where $\xi_n=\left[\frac{\sin\left(n+0.25\right)\pi+\sinh\left(n+0.25\right)\pi}{\cos\left(n+0.25\right)\pi+\cosh\left(n+0.25\right)\pi}\right]$

Clamped-Clamped (CC):

$$\Phi_n(x)=\left\langle \begin{array}{l} \sin\left(\frac{(n+0.5)\pi}{L}x\right)-\sinh\left(\frac{(n+0.5)\pi}{L}x\right)- \\ \xi_n\left[\cos\left(\frac{(n+0.5)\pi}{L}x\right)-\cosh\left(\frac{(n+0.5)\pi}{L}x\right)\right] \end{array} \right\rangle \tag{21}$$

where $\xi_n=\left[\frac{\sin(n+0.5)\pi-\sinh(n+0.5)\pi}{\cos(n+0.5)\pi-\cosh(n+0.5)\pi}\right]$

Multiplying weighting function $\Phi_n(x)$ with Eq. (18) and integrating the weighted residual over the length and letting the integral to zero, we have

$$\int_0^L \Re\Phi_n(x)dx=0\Rightarrow\int_0^L\left[\begin{array}{l} -\tilde{E}(\alpha_1,\beta_1)\frac{\pi}{64}\left(\tilde{d}(\alpha_2,\beta_2)\right)^4\frac{d^4w}{dx^4} \\ +(e_0a)^2\hat{P}\frac{d^4w}{dx^4}-\hat{P}\frac{d^2w}{dx^2} \end{array}\right]\Phi_n(x)dx=0 \tag{22}$$

Now by performing integration by parts, Eq. (22) will be modified into the weak form governing differential equation as

$$\int_0^L\left[\begin{array}{l} -\tilde{E}(\alpha_1,\beta_1)\frac{\pi}{64}\left(\tilde{d}(\alpha_2,\beta_2)\right)^4\frac{d^2\Phi_n(x)}{dx^2}\frac{d^2\Phi_n(x)}{dx^2} \\ +(e_0a)^2\hat{P}\frac{d^2\Phi_n(x)}{dx^2}\frac{d^2\Phi_n(x)}{dx^2}+\hat{P}\frac{d\Phi_n(x)}{dx}\frac{d\Phi_n(x)}{dx} \end{array}\right]dx=0 \tag{23}$$

Simplifying the above Eq.(23), buckling loads $(\hat{P})$ of the nonlocal beam can be obtained as

$$\hat{P}_n=\frac{\int_0^L\tilde{E}(\alpha_1,\beta_1)\frac{\pi}{64}\left(\tilde{d}(\alpha_2,\beta_2)\right)^4\frac{d^2\Phi_n(x)}{dx^2}\frac{d^2\Phi_n(x)}{dx^2}}{\int_0^L\frac{d\Phi_n(x)}{dx}\frac{d\Phi_n(x)}{dx}+(e_0a)^2\frac{d^2\Phi_n(x)}{dx^2}\frac{d^2\Phi_n(x)}{dx^2}} \tag{24}$$

Using the double parametric form as given in Eqs. (12-13), the Eq. (24) will be changed into

$$\hat{P}_n = \frac{\int_0^L \left[\begin{array}{l} \left((e_1 - e_3)\alpha_1\beta_1 + (e_3 - e_1)\beta_1 + (e_2 - e_1)\alpha_1 + e_1\right)\times \\ \left((d_1 - d_3)\alpha_2\beta_2 + (d_3 - d_1)\beta_2 + (d_2 - d_1)\alpha_2 + d_1\right)^4 \end{array} \right] \left(\frac{\pi}{64}\right) \frac{d^2\Phi_n(x)}{dx^2} \frac{d^2\Phi_n(x)}{dx^2}}{\int_0^L \frac{d\Phi_n(x)}{dx}\frac{d\Phi_n(x)}{dx} + (e_0 a)^2 \frac{d^2\Phi_n(x)}{dx^2}\frac{d^2\Phi_n(x)}{dx^2}} \tag{25}$$

4.3 Monte Carlo simulation technique

The uncertain parameters in terms of Triangular Fuzzy Numbers (TFN) are converted into interval form by using a single parametric form presented in Eq. (4) Viz. α cut technique as

$$\tilde{E} = (e_1, e_2, e_3) = \left[\underline{E}(\alpha_1)\ \ \overline{E}(\alpha_1)\right] = \left[(e_2 - e_1)\alpha_1 + e_1\ \ -(e_3 - e_2)\alpha_1 + e_3\right],\ \ \alpha_1 \in [0\ \ 1], \tag{26}$$

$$\tilde{d} = (d_1, d_2, d_3) = \left[\underline{d}(\alpha_2)\ \ \overline{d}(\alpha_2)\right] = \left[(d_2 - d_1)\alpha_2 + d_1\ \ -(d_3 - d_2)\alpha_2 + d_3\right],\ \ \alpha_2 \in [0\ \ 1] \tag{27}$$

10,000 random points have been generated from these intervals and these random points of uncertain parameters are used in the deterministic analysis of critical buckling load. By repeating the deterministic analysis for all the random points, lower bound and upper bound and mean of critical buckling loads are computed. The mean of the critical buckling loads, obtained by the Monte Carlo simulation technique represents the results of the deterministic model.

5. Numerical results and discussion

In this study, critical buckling loads (P_{cr}) of nonlocal beam have been computed for HH, CH and CC boundary conditions by developing MATLAB codes for the proposed uncertain model. The study has progressed by considering three cases (i) Young's modulus (E) is uncertain or fuzzy (ii) diameter (d) is uncertain or fuzzy (iii) Young's modulus (E) and diameter (d) are uncertain or fuzzy. For computational purposes, the structural parameters are considered as, $\tilde{E} = (0.6,\ 1,\ 1.4)\text{TPa}$, where $E = 1\text{TPa}$ is the deterministic value, $\tilde{d} = (0.8, 1, 1.2)\text{nm}$ and $d = 1\text{nm}$ is the deterministic value, $L = 10\text{nm}$, and $I = \frac{\pi \tilde{d}^4}{64}$.

5.1 Validation of the proposed model

The proposed uncertain model is validated by comparing the critical buckling loads with [44] by considering the deterministic values for Young's modulus and diameter. It may be noted that by considering $\alpha_1 = \alpha_2 = 1$, the uncertain models turn into a deterministic model. Critical buckling

loads are compared for HH boundary condition by using Navier's Methods (NM), and Monte Carlo Simulation Technique (MCST) which are depicted in Table 1 and Fig. 4, as tabular and graphical results, respectively. From these results, we may observe a robust agreement between the present results obtained by both the non-probabilistic method and Monte Carlo simulation technique with the existing results of [44].

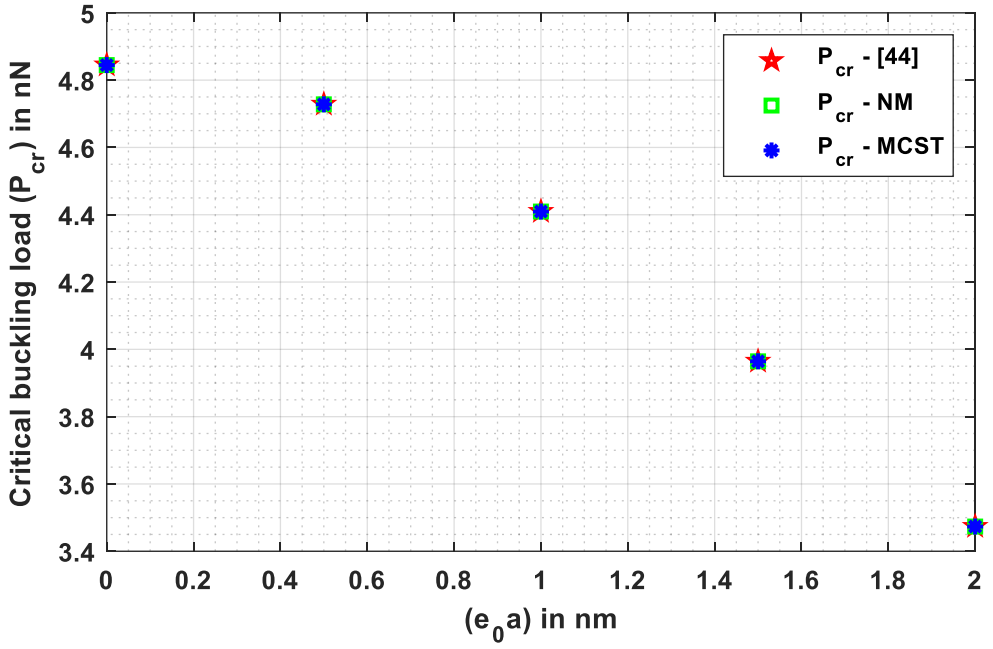

Fig. 4: Comparisons of P_{cr} for HH boundary condition

Table 1: Comparisons of P_{cr} (in nN) for HH boundary condition

(e_0a) in nm	0	0.5	1	1.5	2
P_{cr} - NM (Present)	4.8447	4.7281	4.4095	3.9644	3.4735
P_{cr} -MCST (Present)	4.8447	4.7281	4.4095	3.9644	3.4735
P_{cr} [44]	4.8447	4.7281	4.4095	3.9644	3.4735

5.2 Propagation of uncertainties in critical buckling loads

Through this subsection, propagation of structural uncertainties into dynamical characteristics, in particular, critical buckling loads, have been studied comprehensively. In order to proceed smoothly, three cases have been considered, which are the systems having (i) Young's modulus

(E) as uncertain parameters (ii) diameter (d) as uncertain parameters, and finally (iii) both Young's modulus (E) and diameter (d)as uncertain parameters. It may be noted that double parametric form-based Navier's Method (NM) has been used for HH boundary condition whereas Galerkin Weighted Residual Method has been employed for CH and CC boundary conditions. Also, the random sampling technique based Monte Carlo Simulation Technique is used to compute and verify the results.

The tabular and graphical results for case (i) have been presented in Table 2 and Figs. (5-7), respectively considering the structural parameters as $\tilde{E} = (0.6,\ 1,\ 1.4)$TPa $d = 1nm, e_0 a = 1nm,$ and $L = 10nm$. The critical buckling loads of the uncertain system are being computed through lower bound and upper bound. The tabular results reveal that the results obtained by the non-probabilistic methods and Monte Carlo Simulation Technique are quite agreeing with each other with very little errors. Also, it may be noted that the time taken by Navier's method is quite lesser than the Monte Carlo Simulation Technique. Figs. (5-7) represent the uncertain critical buckling loads in the form Triangular Fuzzy Numbers for HH, CH, and CC boundary conditions, respectively. From these results, it is concluded that the spread of fuzziness or uncertainties in HH boundary is lower whereas, in CC boundary condition, it is comparatively higher.

Table 2: LB and UB of Critical buckling loads (P_{cr}) in nN, considering Young's modulus as an uncertain parameter with $d = 1nm, e_0 a = 1nm,$ and $L = 10nm$.

(a) Hinged-Hinged (HH) boundary condition

α_1	LB of Critical Buckling Load $(\underline{P}_{cr})$			UB of Critical Buckling Load $(\overline{P}_{cr})$		
	NM*	MCST#	% Error	NM*	MCST#	% Error
0	2.6457	2.6457	0	6.1733	6.1732	0.0016
0.1	2.8221	2.8224	0.0106	5.9970	5.9970	0
0.2	2.9985	2.9988	0.0100	5.8206	5.8206	0
0.3	3.1749	3.1749	0	5.6442	5.6434	0.0142
0.4	3.3512	3.3514	0.0060	5.4678	5.4674	0.0073
0.5	3.5276	3.5282	0.0170	5.2914	5.2912	0.0038
0.6	3.7040	3.7041	0.0027	5.1151	5.1144	0.0137

0.7	3.8804	3.8807	0.0077	4.9387	4.9385	0.0040
0.8	4.0568	4.0568	0	4.7623	4.7622	0.0021
0.9	4.2331	4.2332	0.0024	4.5859	4.5859	0
1.0	4.4095	4.4095	0	4.4095	4.4095	0

[#]Time taken for LB and UB by MCST: 67.201382 seconds

[*]Time taken for LB and UB by NM: 3.957473 + 3.895574 = 7.853047seconds

(b) Clamped-Hinged (CH) boundary condition

α_1	LB of Critical Buckling Load $(\underline{P}_{cr})$			UB of Critical Buckling Load $(\overline{P}_{cr})$		
	GWRM[*]	MCST[#]	% Error	GWRM[*]	MCST[#]	% Error
0	5.0399	5.0403	0.0079	11.7597	11.7583	0.0119
0.1	5.3759	5.3762	0.0056	11.4237	11.4227	0.0088
0.2	5.7119	5.7122	0.0053	11.0877	11.0876	0.0009
0.3	6.0479	6.0481	0.0033	10.7517	10.7516	0.0009
0.4	6.3838	6.3843	0.0078	10.4157	10.4156	0.0010
0.5	6.7198	6.7199	0.0015	10.0798	10.0796	0.0020
0.6	7.0558	7.0559	0.0014	9.7438	9.7434	0.0041
0.7	7.3918	7.3919	0.0014	9.4078	9.4069	0.0096
0.8	7.7278	7.7279	0.0013	9.0718	9.0715	0.0033
0.9	8.0638	8.0639	0.0012	8.7358	8.7358	0
1.0	8.3998	8.3998	0	8.3998	8.3998	0

[#]Time taken for LB and UB by MCST: 1021.220816 seconds

[*]Time taken for LB and UB by GWRM: 6.889991 + 6.766945=13.656936 seconds

(c) Clamped-Clamped (CC) boundary condition

α_1	LB of Critical Buckling Load $(\underline{P}_{cr})$			UB of Critical Buckling Load $(\overline{P}_{cr})$		
	GWRM*	MCST#	% Error	GWRM*	MCST#	% Error
0	8.3825	8.3835	0.0119	19.5592	19.5584	0.0041
0.1	8.9414	8.9422	0.0089	19.0004	19.0003	0.0005
0.2	9.5002	9.5009	0.0074	18.4416	18.4405	0.0060
0.3	10.0590	10.0616	0.0258	17.8827	17.8813	0.0078
0.4	10.6179	10.6180	0.0009	17.3239	17.3236	0.0017
0.5	11.1767	11.1774	0.0063	16.7650	16.7649	0.0006
0.6	11.7355	11.7360	0.0043	16.2062	16.2061	0.0006
0.7	12.2944	12.2950	0.0049	15.6474	15.6470	0.0026
0.8	12.8532	12.8535	0.0023	15.0885	15.0884	0.0007
0.9	13.4120	13.4122	0.0015	14.5297	14.5296	0.0007
1.0	13.9709	13.9709	0	13.9709	13.9709	0

#Time taken for LB and UB by MCST: 789.324982 seconds

*Time taken for LB and UB by GWRM: 6.618879 + 6.595867 =13.214746 seconds

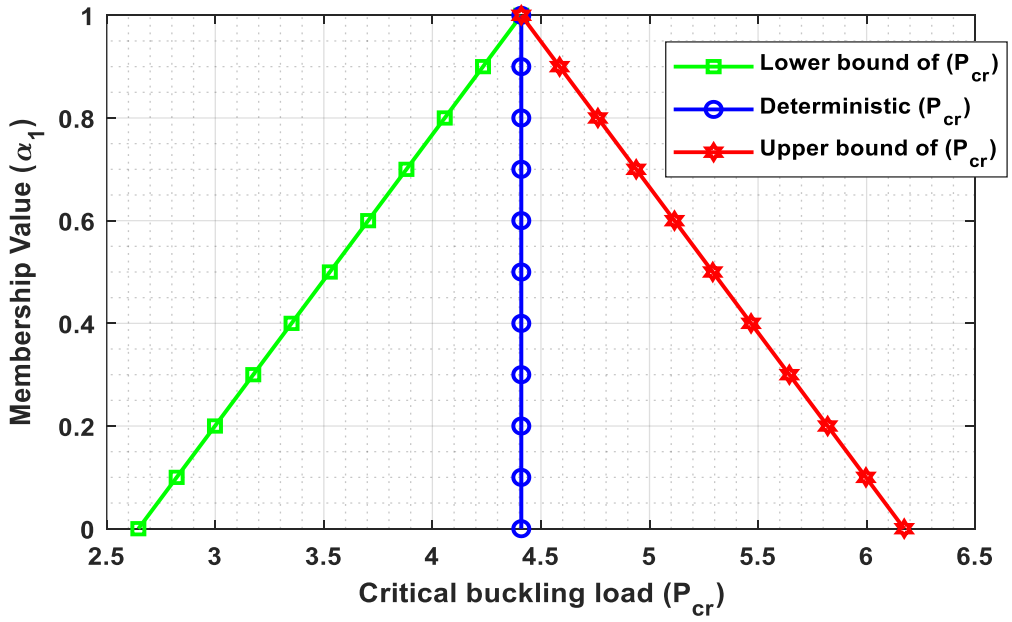

Fig. 5: TFN of P_{cr} for HH boundary condition when E is an uncertain parameter

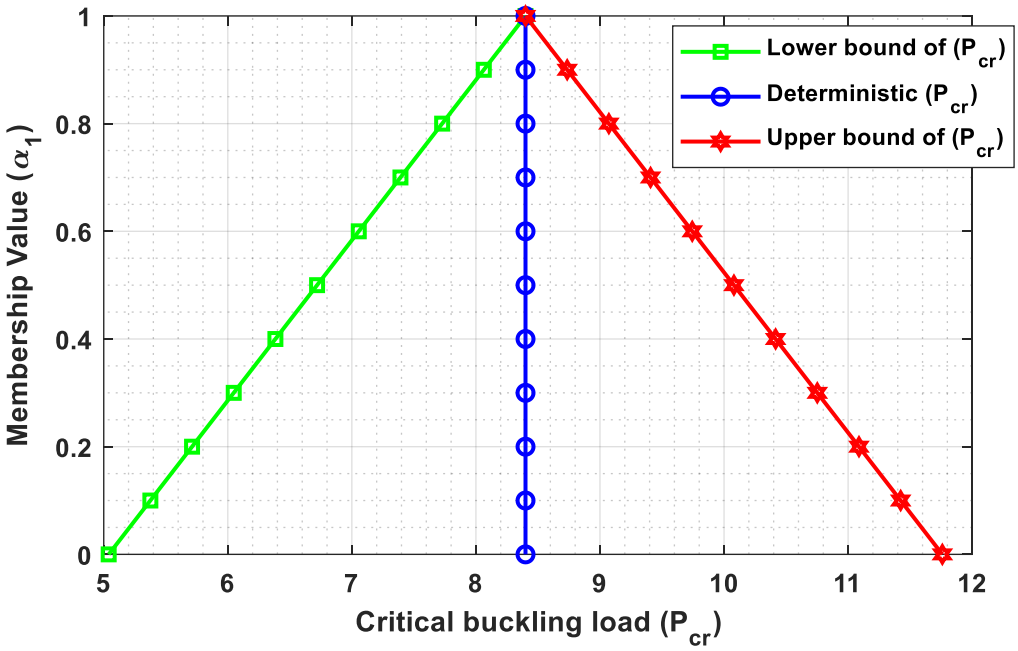

Fig. 6: TFN of P_{cr} for CH boundary condition when E is an uncertain parameter

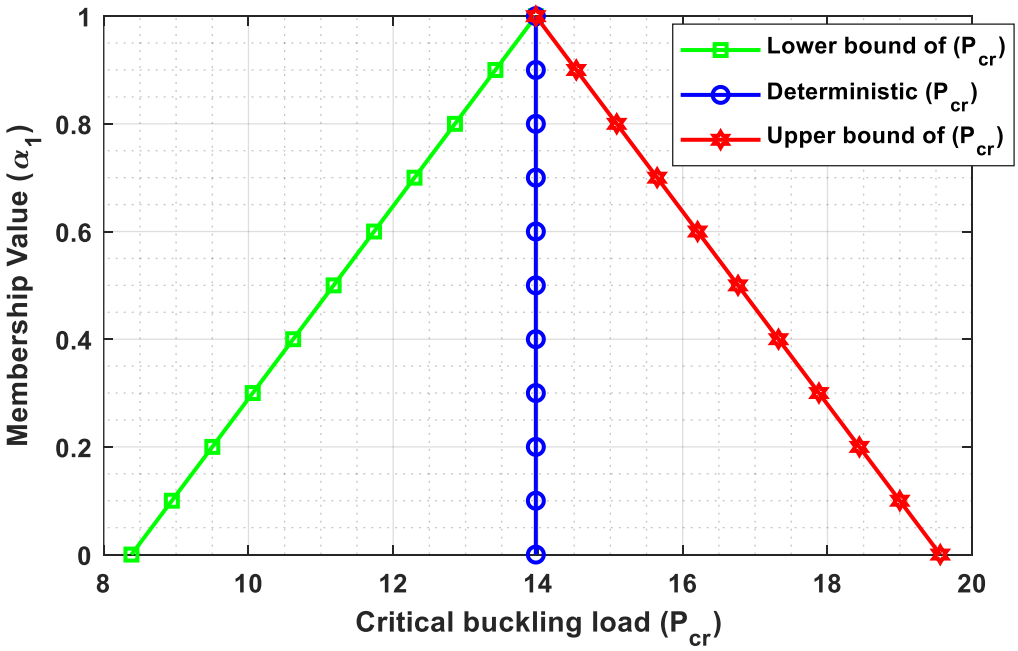

Fig. 7: TFN of P_{cr} for CC boundary condition when E is an uncertain parameter

Table 3 and Figs. (8-10) demonstrate the tabular and graphical results for the second case where the diameter of the nonlocal beam has been considered as uncertain considering the structural parameters as $\tilde{d} = (0.8, 1, 1.2)\text{nm}$, $E = 1TPa, e_0 a = 1nm,$ and $L = 10nm$. In the second case, the tabular results obtained by the non-probabilistic methods are also matching with the results obtained by Monte Carlo Simulation Technique. Also, the time taken by Navier's method is very less than that of the Monte Carlo Simulation Technique. Figs. (8-10) represent the critical buckling loads in the form Triangular Fuzzy Numbers for HH, CH, and CC boundary conditions, respectively. The propagation of uncertainties to the critical buckling loads with respect to the uncertain diameter is higher in case of Clamped- Clamped edge and lower in case of Hinged-Hinged edge.

Table 3: LB and UB of Critical buckling loads (P_{cr}) in nN, considering diameter as an uncertain parameter with $E = 1TPa, e_0 a = 1nm,$ and $L = 10nm$.

(a) Hinged-Hinged (HH) boundary condition

α_2	LB of Critical Buckling Load $(\underline{P}_{cr})$			UB of Critical Buckling Load $(\overline{P}_{cr})$		
	NM*	MCST#	% Error	NM*	MCST#	% Error
0	1.8061	1.8067	0.0332	9.1436	9.1400	0.0394
0.1	1.9936	1.9952	0.0803	8.5491	8.5490	0.0012
0.2	2.1954	2.1955	0.0046	7.9841	7.9808	0.0413
0.3	2.4120	2.4124	0.0166	7.4475	7.4459	0.0215
0.4	2.6444	2.6444	0	6.9385	6.9383	0.0029
0.5	2.8931	2.8931	0	6.4560	6.4560	0
0.6	3.1590	3.1596	0.0190	5.9991	5.9981	0.0167
0.7	3.4427	3.4428	0.0029	5.5669	5.5667	0.0036
0.8	3.7452	3.7455	0.0080	5.1585	5.1584	0.0019
0.9	4.0672	4.0674	0.0049	4.7730	4.7730	0
1.0	4.4095	4.4095	0	4.4095	4.4095	0

[#]Time taken for LB and UB by MCST: 51.188114 seconds

[*]Time taken for LB and UB by NM: 3.876123 + 3.921826 =7.797949 seconds

(b) Clamped-Hinged (CH) boundary condition

α_2	LB of Critical Buckling Load $(\underline{P}_{cr})$			UB of Critical Buckling Load $(\overline{P}_{cr})$		
	GWRM[*]	MCST[#]	% Error	GWRM[*]	MCST[#]	% Error
0	3.4406	3.4417	0.0320	17.4178	17.4110	0.0390
0.1	3.7977	3.8007	0.0790	16.2853	16.2852	0.0006
0.2	4.1820	4.1822	0.0048	15.2090	15.2027	0.0414
0.3	4.5948	4.5955	0.0152	14.1869	14.1837	0.0226
0.4	5.0373	5.0374	0.0020	13.2172	13.2169	0.0023
0.5	5.5111	5.5112	0.0018	12.2981	12.2981	0
0.6	6.0176	6.0187	0.0183	11.4278	11.4259	0.0166
0.7	6.5581	6.5583	0.0030	10.6045	10.6042	0.0028
0.8	7.1343	7.1348	0.0070	9.8266	9.8264	0.0020
0.9	7.7477	7.7481	0.0052	9.0922	9.0921	0.0011
1.0	8.3998	8.3998	0	8.3998	8.3998	0

[#]Time taken for LB and UB by MCST: 1028.984054 seconds

[*]Time taken for LB and UB by GWRM: 6.757198 + 6.849629 =13.606827 seconds

(c) Clamped-Clamped (CC) boundary condition

α_1	LB of Critical Buckling Load $(\underline{P}_{cr})$			UB of Critical Buckling Load $(\overline{P}_{cr})$		
	GWRM[*]	MCST[#]	% Error	GWRM[*]	MCST[#]	% Error
0	5.7225	5.7227	0.0035	28.9700	28.9600	0.0345
0.1	6.3165	6.3166	0.0016	27.0864	27.0829	0.0129
0.2	6.9557	6.9558	0.0014	25.2962	25.2953	0.0036
0.3	7.6422	7.6425	0.0039	23.5962	23.5960	0.0008
0.4	8.3783	8.3794	0.0131	21.9834	21.9813	0.0096

0.5	9.1663	9.1664	0.0011	20.4548	20.4506	0.0205
0.6	10.0086	10.0092	0.0060	19.0072	19.0067	0.0026
0.7	10.9077	10.9095	0.0165	17.6379	17.6379	0
0.8	11.8661	11.8662	0.0008	16.3439	16.3439	0
0.9	12.8863	12.8865	0.0016	15.1225	15.1218	0.0046
1.0	13.9709	13.9709	0	13.9709	13.9709	0

[#]Time taken for LB and UB by MCST: 792.197172 seconds

[*]Time taken for LB and UB by GWRM: 6.630419 + 6.642321 =13.27274 seconds

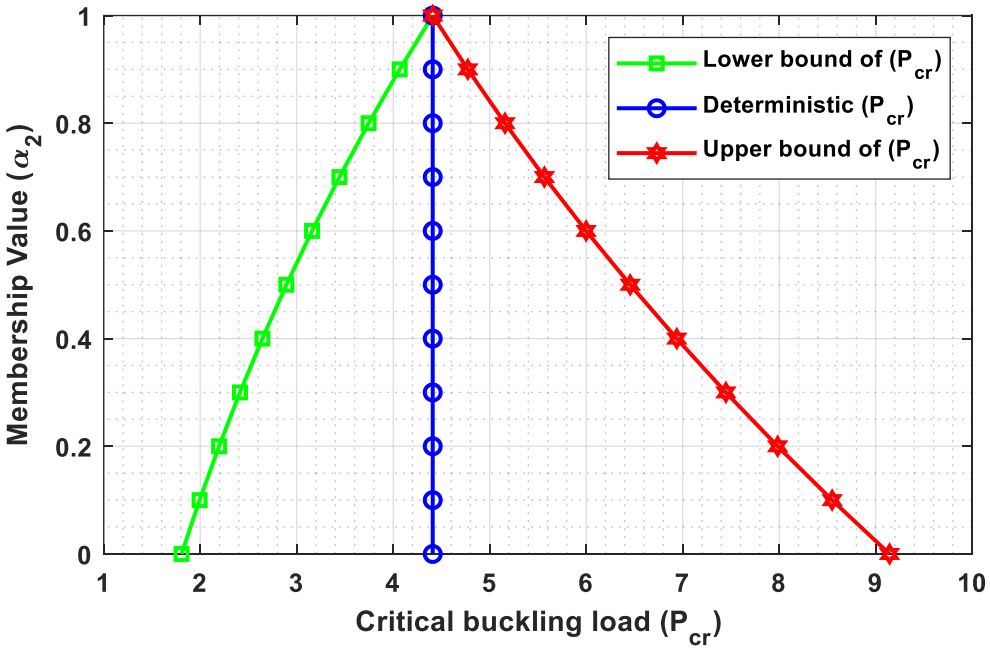

Fig. 8: TFN of P_{cr} for HH boundary condition when d is an uncertain parameter

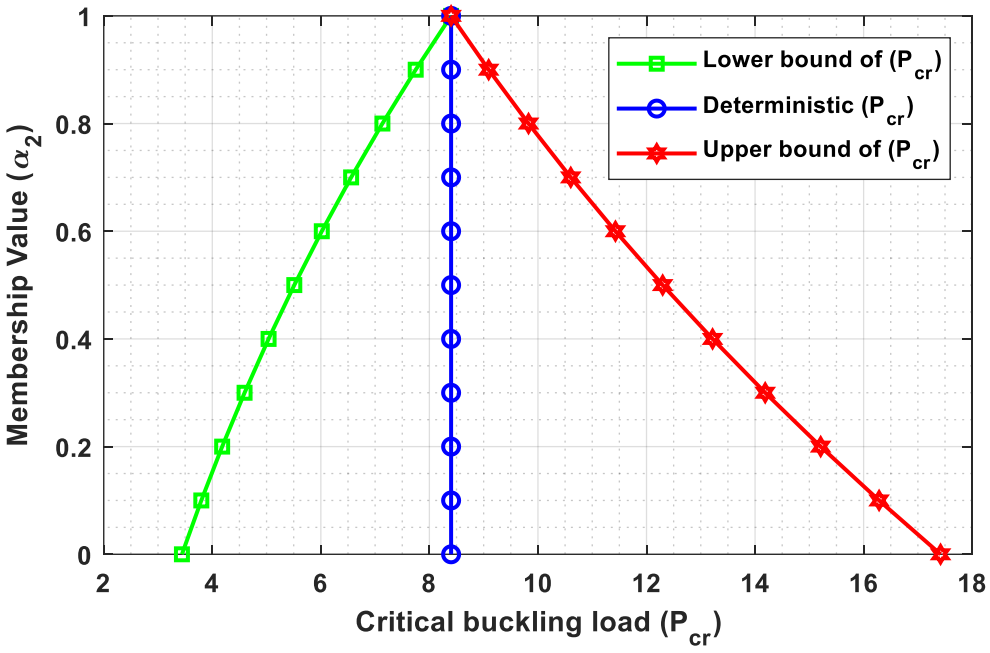

Fig. 9: TFN of P_{cr} for CH boundary condition when d is an uncertain parameter

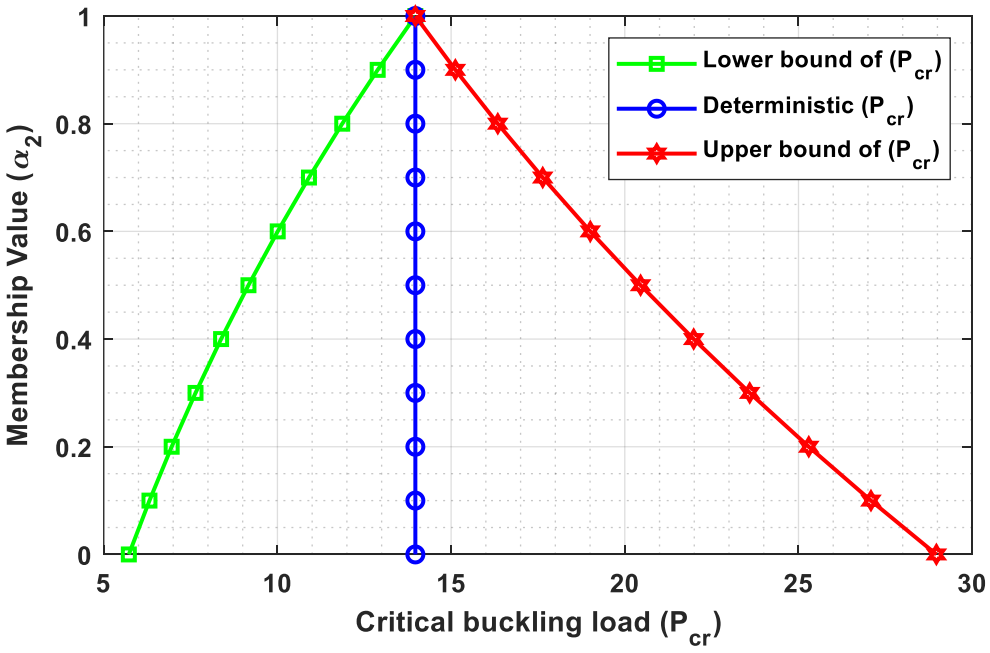

Fig. 10: TFN of P_{cr} for CC boundary condition when d is an uncertain parameter

Likewise, Table 4 and Figs. (11-13) are the tabular and graphical results of critical buckling loads where both Young's modulus and the diameter of the beam have been assumed as uncertain parameters with $\tilde{E} = (0.6,\ 1,\ 1.4)\text{TPa}$, $\tilde{d} = (0.8, 1, 1.2)\text{nm}$, $e_0 a = 1nm$, and $L = 10nm$. In this case, the tabular results are obtained by the non-probabilistic methods as the time taken to compute the critical buckling loads by Monte Carlo Simulation Technique is very high. Figs. (11-13) are the uncertain critical buckling loads in the form Triangular Fuzzy Numbers for HH, CH, and CC boundary conditions, respectively.

The critical buckling loads for the uncertain systems in terms of Triangular Fuzzy Numbers are also compared for each boundary condition considering all the three cases in the form of graphical results which are given in Figs. (14-16). Fig. 14 represents the comparison for HH boundary condition whereas Fig. 15 and Fig. 16 demonstrate for CH and CC boundary conditions respectively. From these figures, it can be observed that the spread of fuzziness or uncertainties in critical buckling load is comparatively less when Young's modulus is uncertain than that of uncertain diameter and uncertain Young's modulus and diameter. This is because uncertainties in Young's modulus and diameter are propagating to critical buckling load with a comparatively larger extent than that of uncertain Young's modulus and uncertain diameter. This trend is true for all the three boundary conditions

Table 4: LB and UB of Critical buckling loads (P_{cr}) in nN, considering both Young's modulus and diameter as uncertain parameters with $e_0 a = 1nm$, and $L = 10nm$.

$\alpha_1 = \alpha_2$	LB of Critical Buckling Load $(\underline{P}_{cr})$			UB of Critical Buckling Load $(\overline{P}_{cr})$		
	HH	CH	CC	HH	CH	CC
0	1.0837	2.0643	3.4335	12.8010	24.3849	40.5580
0.1	1.2759	2.4305	4.0426	11.6268	22.1480	36.8375
0.2	1.4929	2.8438	4.7299	10.5390	20.0759	33.3910
0.3	1.7367	3.3082	5.5024	9.5328	18.1593	30.2032
0.4	2.0097	3.8284	6.3675	8.6037	16.3894	27.2595
0.5	2.3145	4.4089	7.3330	7.7472	14.7578	24.5457
0.6	2.6535	5.0547	8.4073	6.9590	13.2563	22.0484
0.7	3.0296	5.7712	9.5988	6.2350	11.8771	19.7545

0.8	3.4456	6.5636	10.9168	5.5712	10.6127	17.6515
0.9	3.9045	7.4378	12.3708	4.9639	9.4559	15.7274
1.0	4.4095	8.3998	13.9709	4.4095	8.3998	13.9709

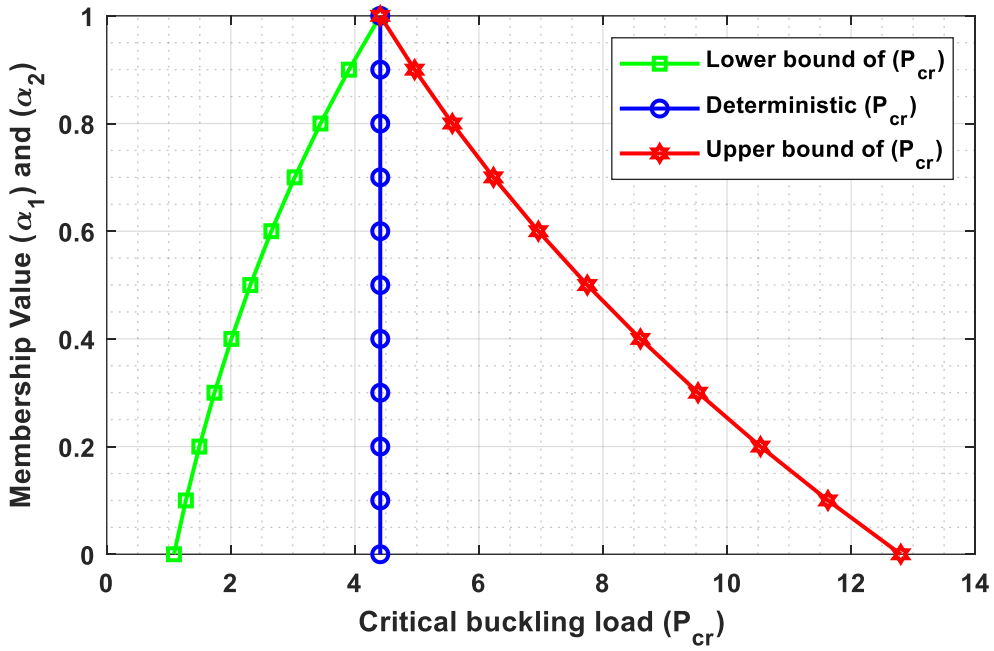

Fig. 11: TFN of P_{cr} for HH boundary condition when E and d are uncertain parameters

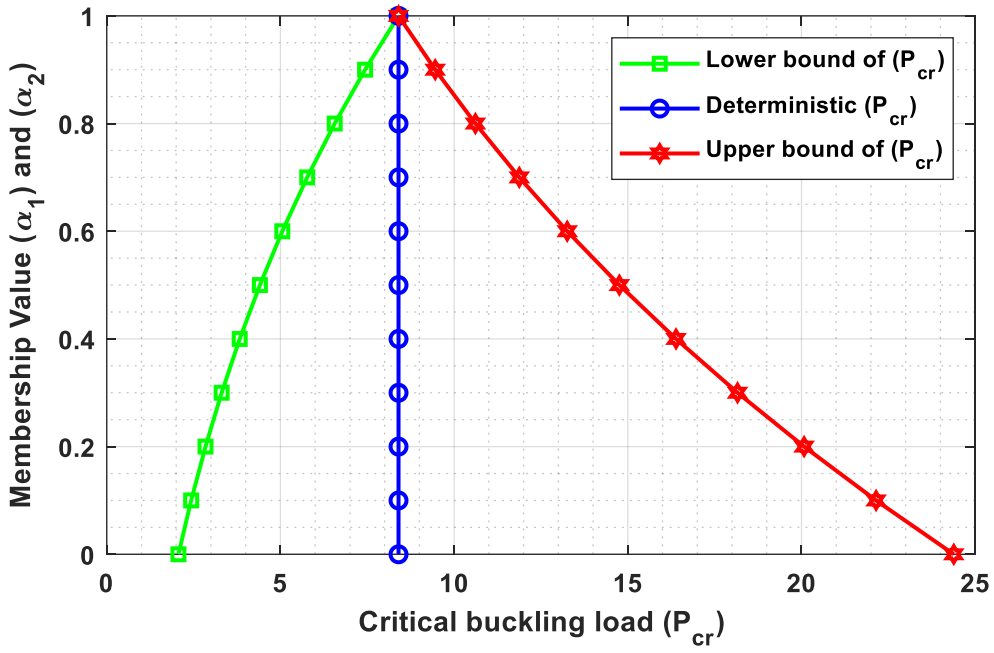

Fig. 12: TFN of P_{cr} for CH boundary condition when E and d are uncertain parameters

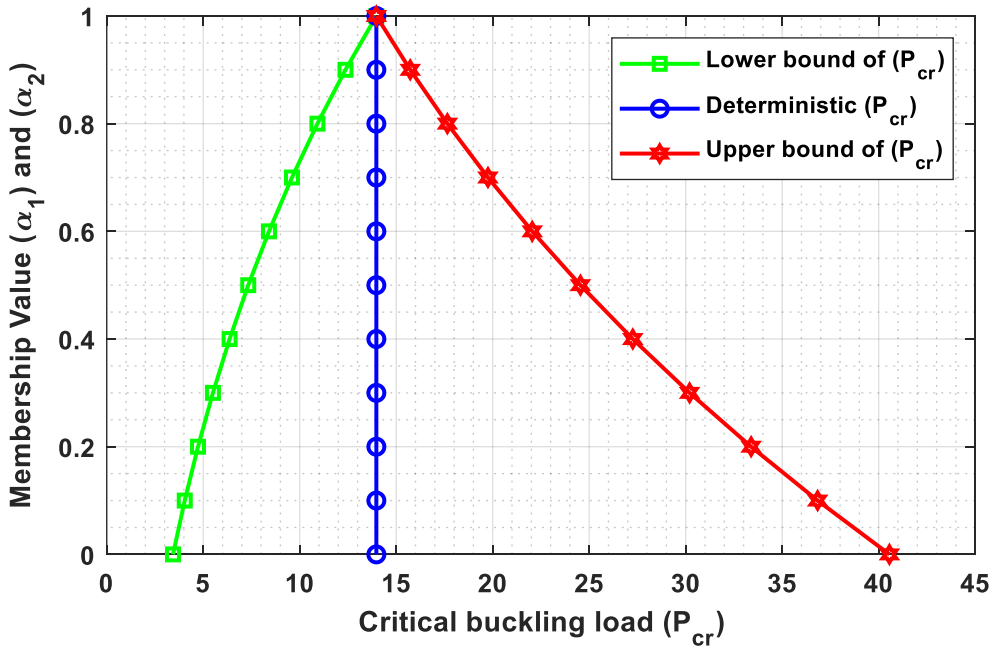

Fig. 13: TFN of P_{cr} for CC boundary condition when E and d are uncertain parameters

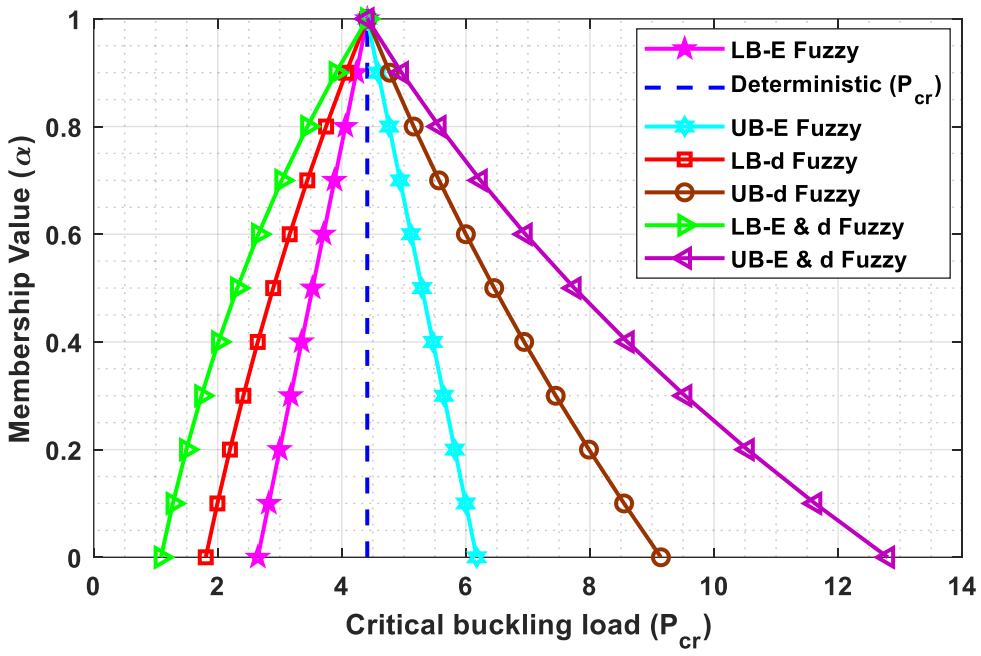

Fig. 14: Comparisons of TFN of P_{cr} for HH boundary condition

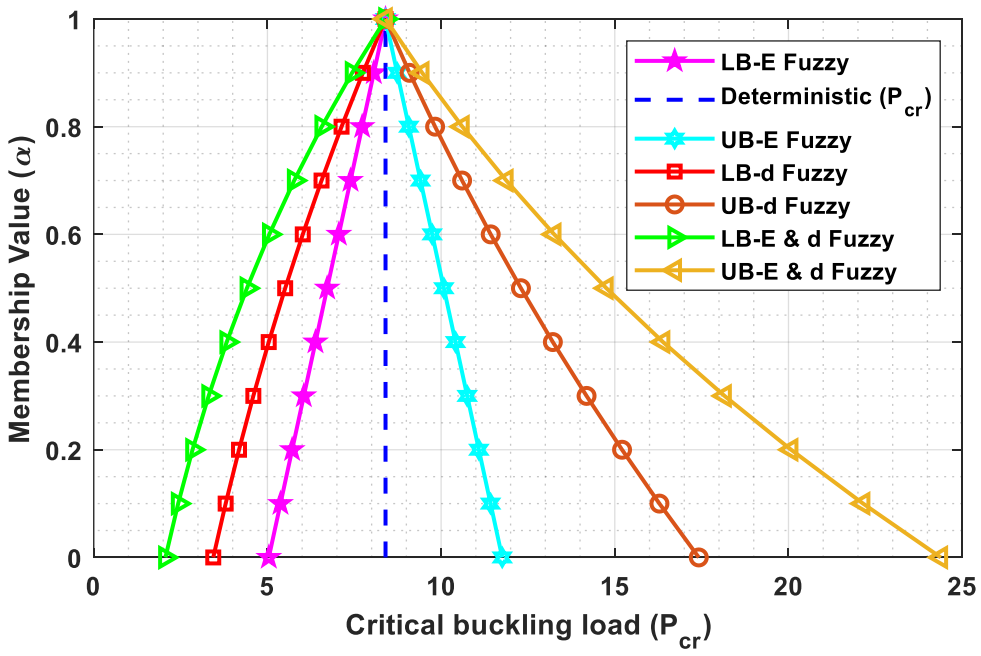

Fig. 15: Comparisons of TFN of P_{cr} for CH boundary condition

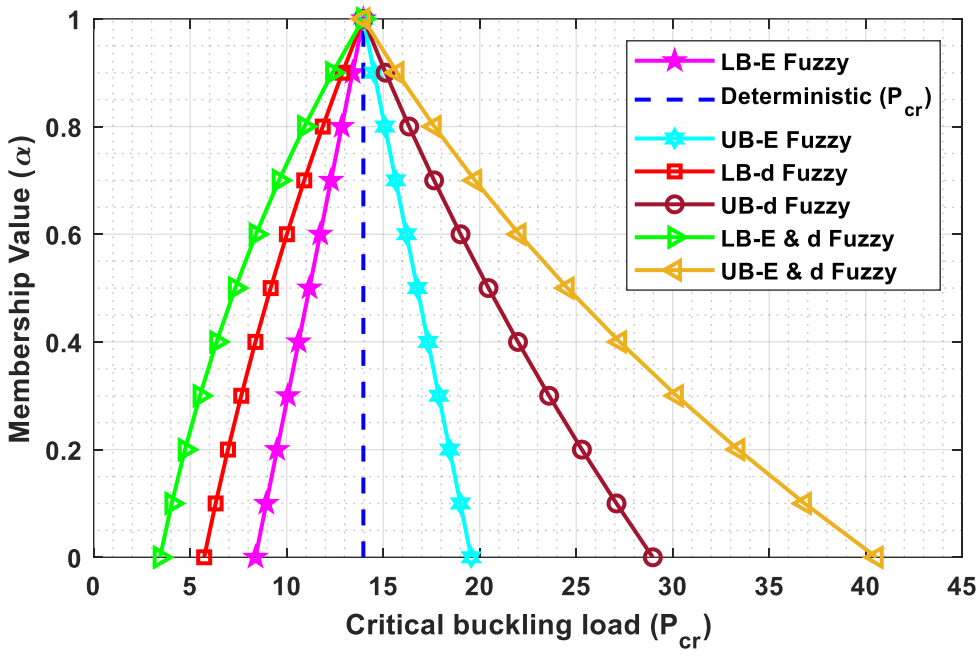

Fig. 16: Comparisons of TFN of P_{cr} for CC boundary condition

6. Concluding remarks

In this study, Euler- Bernoulli nanobeam is modeled with material uncertainties by considering Young's modulus and diameter of the beam as uncertain parameters. The material uncertainties are considered here as fuzzy numbers, in particular, Triangular fuzzy numbers. In this scenario, the double parametric form has been used to handle the fuzzy uncertainty and the two parameters control the behavior of the uncertainty. Two non-probabilistic methods such as double parametric form-based Navier's Method (NM) and Galerkin Weighted Residual Method (GWRM) have been proposed and employed to calculate the critical buckling loads of nonlocal beam. It is also worth mentioning that this form may also give direct results for crisp and interval cases. Although the numerical methods have to be developed by taking care of the double parametric form of the fuzzy numbers, the results may be obtained in general form having the essence of the uncertainties. Three boundary conditions such as Hinged-Hinged (HH), Clamped-Hinged (CH), and Clamped-Clamped (CC) have been considered in this study. Further, a random sampling technique based method namely, Monte Carlo Simulation Technique (MCST) has been implemented to compute the critical buckling loads of uncertain systems. The results obtained by non-probabilistic methods

are compared with both the deterministic model in special cases and uncertain models, demonstrating robust agreement. The time taken by the non-probabilistic methods for the computation of critical buckling loads is very less as compared to the Monte Carlo Simulation Technique (MCST), showing the effectiveness of the methods with respect to time. Additionally, a parametric study has been performed to display the propagation of uncertainties into the nonlocal system in the form of critical buckling loads. It may be also noted that the spread of uncertainties when Young's modulus is uncertain is comparatively less whereas the spread is high when both Young's modulus and diameter are uncertain that means, higher the uncertainties in structural parameters leads to the higher spread of critical buckling loads.

Acknowledgment

The first two authors would like to acknowledge Defence Research & Development Organization (DRDO), New Delhi, India (Sanction Code: DG/TM/ERIPR/GIA/17-18/0129/020) for the funding to carry out the present research work.

References

[1] Liu H, Zhang W, Yuan H (2016) Structural stability analysis of single-layer reticulated shells with stochastic imperfections. Engineering Structures 124:473-479

[2] Liu H, Lv Z (2018) Vibration and instability analysis of flow-conveying carbon nanotubes in the presence of material uncertainties. Physica A: Statistical Mechanics and its Applications 511:85-103

[3] Alon N, Spencer JH (2000) The probabilistic method. John Wiley & Sons, New York

[4] Malikan M, Nguyen VB, Tornabene F (2018) Damped forced vibration analysis of single-walled carbon nanotubes resting on viscoelastic foundation in thermal environment using nonlocal strain gradient theory. Engineering Science and Technology, an International Journal 21:778-786

[5] Malikan M (2019) On the buckling response of axially pressurized nanotubes based on a novel nonlocal beam theory. Journal of Applied and Computational Mechanics 5:103-112

[6] Malikan M, Dimitri R, Tornabene F (2019) Transient response of oscillated carbon nanotubes with an internal and external damping. Composites Part B: Engineering 158:198-205

[7] Sobhy M (2015) Thermoelastic response of FGM plates with temperature-dependent properties resting on variable elastic foundations. International Journal of Applied Mechanics 7(06):1550082

[8] Karami B, Janghorban M, Tounsi A (2019) Galerkin's approach for buckling analysis of functionally graded anisotropic nanoplates/different boundary conditions. Engineering with Computers 35(4):1297-1316

[9] Salvetat JP, Briggs GA, Bonard JM, Bacsa RR, Kulik AJ, Stöckli T, Burnham NA, Forró L (1999) Elastic and shear moduli of single-walled carbon nanotube ropes. Physical review letters 82:944

[10] Krishnan A, Dujardin E, Ebbesen TW, Yianilos PN, Treacy MM (1998) Young's modulus of single-walled nanotubes. Physical review B 58:14013

[11] He L, Guo S, Lei J, Sha Z, Liu Z (2014) The effect of Stone–Thrower–Wales defects on mechanical properties of graphene sheets–A molecular dynamics study. Carbon 75:124-32

[12] Radebe IS, Adali S (2014) Buckling and sensitivity analysis of nonlocal orthotropic nanoplates with uncertain material properties. Composites Part B: Engineering 56:840-886

[13] Lv Z, Liu H (2017) Nonlinear bending response of functionally graded nanobeams with material uncertainties. International Journal of Mechanical Sciences 134:123–135

[14] Lv Z, Liu H (2018) Uncertainty modeling for vibration and buckling behaviors of functionally graded nanobeams in thermal environment. Composite Structures 184:1165–1176

[15] Liu H, Lv Z (2018) Uncertain material properties on wave dispersion behaviors of smart magneto-electro-elastic nanobeams. Composite Structures 202:615–624

[16] Liu H, Lv Z (2018) Vibration and instability analysis of flow-conveying carbon nanotubes in the presence of material uncertainties. Physica A: Statistical Mechanics and its Applications 511: 85-103

[17] Liu H, Lv Z (2018) Uncertainty analysis for wave dispersion behavior of carbon nanotubes embedded in Pasternak-type elastic medium. Mechanics Research Communications 92:92-100

[18] Jena SK, Chakraverty S, Jena RM (2019) Propagation of uncertainty in free vibration of Euler–Bernoulli nanobeam. Journal of the Brazilian Society of Mechanical Sciences and Engineering 41:436

[19] Gironacci E, Nezhad MM, Rezania M, Lancioni G (2018) A non-local probabilistic method for modeling of crack propagation. International Journal of Mechanical Sciences 144:897–908

[20] Zhu J, Lv Z, Liu H (2019) Thermo-electro-mechanical vibration analysis of nonlocal piezoelectric nanoplates involving material uncertainties. Composite Structures 208:771–783

[21] Karami B, Shahsavari D (2020) On the forced resonant vibration analysis of functionally graded polymer composite doubly-curved nanoshells reinforced with graphene-nanoplatelets. Computer Methods in Applied Mechanics and Engineering 359:112767

[22] Karami B, Janghorban M, Rabczuk T (2020) Dynamics of two-dimensional functionally graded tapered Timoshenko nanobeam in thermal environment using nonlocal strain gradient theory. Composites Part B: Engineering 182:107622

[23] Karami B, Janghorban M, Tounsi A (2020) Novel study on functionally graded anisotropic doubly curved nanoshells. The European Physical Journal Plus 135(1):103

[24] Karami B, Janghorban M, Tounsi A (2019) On pre-stressed functionally graded anisotropic nanoshell in magnetic field. Journal of the Brazilian Society of Mechanical Sciences and Engineering 41(11):495

[25] Karami B, Shahsavari D, Janghorban M, Li L (2019) On the resonance of functionally graded nanoplates using bi-Helmholtz nonlocal strain gradient theory. International Journal of Engineering Science 144:103143

[26] Karami B, Janghorban M, Rabczuk T (2019) Static analysis of functionally graded anisotropic nanoplates using nonlocal strain gradient theory. Composite Structures 227:111249

[27] Lyu Z, Yang Y, Liu H (2020) High-accuracy hull iteration method for uncertainty propagation in fluid-conveying carbon nanotube system under multi-physical fields. Applied Mathematical Modelling 79:362-80

[28] Liu H, Lv Z, Wu H (2019) Nonlinear free vibration of geometrically imperfect functionally graded sandwich nanobeams based on nonlocal strain gradient theory. Composite Structures 214:47-61

[29] Liu H, Wu H, Lyu Z (2020) Nonlinear resonance of FG multilayer beam-type nanocomposites: Effects of graphene nanoplatelet-reinforcement and geometric imperfection. Aerospace Science and Technology 105702

[30] Malikan M, Eremeyev VA (2020) Post-critical buckling of truncated conical carbon nanotubes considering surface effects embedding in a nonlinear Winkler substrate using the Rayleigh-Ritz method. Materials Research Express 7(2): 025005

[31] Malikan M, Krasheninnikov M, Eremeyev VA (2020) Torsional stability capacity of a nano-composite shell based on a nonlocal strain gradient shell model under a three-dimensional magnetic field. International Journal of Engineering Science 148:103210

[32] Jena SK, Chakraverty S, Malikan M (2020) Vibration and buckling characteristics of nonlocal beam placed in a magnetic field embedded in Winkler–Pasternak elastic foundation using a new refined beam theory: an analytical approach. The European Physical Journal Plus 135(2):164

[33] Jena SK, Chakraverty S, Malikan M, Tornabene F (2019) Stability analysis of single-walled carbon nanotubes embedded in winkler foundation placed in a thermal environment considering the surface effect using a new refined beam theory. Mechanics Based Design of Structures and Machines 1-5

[34] Jena SK, Chakraverty S (2019) Dynamic Behavior of Electro-Magnetic Nanobeam Using Haar Wavelet Method (HWM) and Higher Order Haar Wavelet Method (HOHWM). The European Physical Journal Plus 134(10):538

[35] Jena SK, Chakraverty S, Tornabene F (2019) Buckling Behavior of Nanobeam Placed in an Electro-Magnetic Field Using Shifted Chebyshev polynomials Based Rayleigh-Ritz Method. Nanomaterials 9(9): 1326

[36] Jena SK, Chakraverty S, Malikan M (2019) Implementation of Haar wavelet, higher order Haar wavelet, and differential quadrature methods on buckling response of strain gradient nonlocal beam embedded in an elastic medium. Engineering with Computers https://doi.org/10.1007/s00366-019-00883-1

[37] Jena SK, Chakraverty S, Jena RM, Tornabene F (2019) A novel fractional nonlocal model and its application in buckling analysis of Euler-Bernoulli nanobeam. Materials Research Express 6:055016

[38] Jena SK, Chakraverty S, Tornabene F (2019) Vibration characteristics of nanobeam with exponentially varying flexural rigidity resting on linearly varying elastic foundation using differential quadrature method. Materials Research Express 6:085051

[39] Jena SK, Chakraverty S, Tornabene F (2019) Dynamical behavior of nanobeam embedded in constant, linear, parabolic, and sinusoidal types of Winkler elastic foundation using First-Order nonlocal strain gradient model. Materials Research Express 6:0850f2

[40] Jena SK, Chakraverty S (2018) Free vibration analysis of variable cross-section single layered graphene nano-ribbons (SLGNRs) using differential quadrature method. Frontiers in Built Environment 4:63

[41] Jena SK, Chakraverty S (2018) Free vibration analysis of single walled carbon nanotube with exponentially varying stiffness. Curved and Layered Structures 5:201-212

[42] Jena SK, Chakraverty S (2018) Free vibration analysis of Euler-Bernoulli Nano beam using differential transform method. International Journal of Computational Materials Science and Engineering 7:1850020

[43] Chakraverty S, Jena SK (2018) Free vibration of single walled carbon nanotube resting on exponentially varying elastic foundation. Curved and Layered Structures 5:260-272

[44] Wang CM, Zhang YY, Ramesh SS, Kitipornchai S (2006) Buckling analysis of micro-and nano-rods/tubes based on nonlocal Timoshenko beam theory. J. Phys. D: Appl. Phys. 39: 3904

[45] Jena SK, Chakraverty S (2019) Differential Quadrature and Differential Transformation Methods in Buckling Analysis of Nanobeams. Curved and Layered Structures 6:68-76

[46] Jena SK, Chakraverty S (2019) Dynamic Analysis of Single-Layered Graphene Nano-Ribbons (SLGNRs) with Variable Cross-Section Resting on Elastic Foundation. Curved and Layered Structures 6(1):132-145

[47] Jena SK, Chakraverty S (2020) Vibration Analysis of Nonuniform Single-Walled Carbon Nanotube Resting on Winkler Elastic Foundation Using DQM. In Recent Trends in Wave Mechanics and Vibrations 371-391. Springer, Singapore

[48] Jena RM, Chakraverty S, Jena SK (2019) Dynamic response analysis of fractionally damped beams subjected to external loads using Homotopy Analysis Method. Journal of Applied and Computational Mechanics 5:355-366

[49] Zadeh L (1965) Fuzzy sets. Inf Control 8(3):338–353

[50] Cherki A, Plessis G, Lallemand B, Tison T, Level (2000) P. Level, Fuzzy behavior of mechanical systems with uncertain boundary conditions. Computer Methods in Applied Mechanics and Engineering 189 :863-873

[51] Wasfy TM, Noor AK (1998) Application of fuzzy sets to transient analysis of space structures. Finite Elements in Analysis and Design 29:153-171

[52] Akpan UO, Koko TS, Orisamolu IR, Gallant BK (2000) Fuzzy finite-element analysis of smart structures. Smart Materials and Structures 10:273

[53] Tapaswini S, Chakraverty S (2014) Dynamic response of imprecisely defined beam subject to various loads using Adomian decomposition method. Appl Soft Comput 24:249–263

[54] Michael H (2005) Applied fuzzy arithmetic an introduction with engineering applications

[55] Chakraverty S, Tapaswini S, Behera D (2016) Fuzzy differential equations and applications for engineers and scientists. CRC Press, Boca Raton

[56] Chakraverty S, Tapaswini S, Behera D (2016) Fuzzy arbitrary order system: fuzzy fractional differential equations and applications. Wiley, Hoboken

[57] Reddy JN (2007) Nonlocal theories for bending, buckling and vibration of beams. International Journal of Engineering Science 45: 288-307

[58] Eringen AC (1972) Nonlocal polar elastic continua. Internat. J. Engrg. Sci. 10: 1–16